of **7** (114.5 (4)°), it should be recalled that the three-membered hydrocarbon ring in **6b** widens the seven-membered ring pseudoboat, thus opening the SiOC angle.

It is interesting that the metric parameter with the greatest flexibility among these structures is the oxygen angle, since the Si-O bond distances (1.62-1.63 Å) and the OSiO angles (107-110°) appear to be quite constant within experimental error.

Acknowledgment. We are grateful to the National Science Foundation for support of this research and to Y. Su for assistance in the molecular mechanics calculations.

Supplementary Material Available: Tables of anisotropic thermal parameters, bond lengths, and bond angles for **6a**, **6b**, and **7** (9 pages); tables of calculated and observed structure factors for **6a**, **6b**, and **7** (11 pages). Ordering information is given on any current masthead page.

Contribution from Lash Miller Chemical Laboratories, Department of Chemistry, University of Toronto, Toronto, Ontario M5S 1A1, Canada, and AT&T Bell Laboratories, 600 Mountain Avenue, Murray Hill, New Jersey 07974

Liquid-Phase Metal Vapor Chemistry: Rotary Reactors and Electron-Beam Evaporation Sources

G. A. Ozin,*[,†] M. P. Andrews,*[,‡] C. G. Francis,[†] H. X. Hüber,[†] and K. Molnar[†]

Received March 21, 1989

A new rotatable metal atom reactor that allows electron-beam vaporizations of refractory materials into liquid solutions at reduced temperatures is described. This innovation demonstrably broadens the scope of synthesis from metal atoms and molecular high-temperature species. Details of the instrument and its operation are provided, together with results of studies of charged particle emissions, a description of techniques for quantifying the rate of metal atom deposition, and a description of a variable-temperature transfer tube for removing thermally labile compounds. A simple addition of the furnace that substantially reduces the power required to evaporate even the most refractory elements leads to dramatically increased vaporization rates for modestly powered 2-kW guns. The paper concludes with some test applications of the device in the liquid-phase electron-beam synthesis of some bis(η^6-arene) complexes of titanium, vanadium, and molybdenum.

1. Introduction

In his book on the condensed-phase reactions of high-temperature species, Klabunde[1] remarks on the need to perfect electron-beam equipment suitable for metal vapor synthesis (MVS). A notable innovation in this area has been the development of the reverse-polarity electron gun by Green and coworkers.[2] This device employs a positive hearth (anode) with an unearthed electrostatic focusing shield. With these modifications the primary (incident) electrons are focused on and confined by the positive hearth. Secondary electrons scattered from the molten metal are suppressed in numbers, with emission levels reduced by 3 orders of magnitude (milliamps to microamps). Reagent damage decreases as a result. Accompanying ion emissions from this device are small (microamps) and tolerable in a synthetic sense.[2]

Changing requirements in the field of metal vapor synthesis have stimulated efforts to extend the range of applicability of electron-beam technology to liquid-phase reaction chemistry, to quantify the metal atom deposition process, and to incorporate multivaporization sources in multimetallic applications.[3] In turn, these adaptations make the hardware more flexible for use in inorganic, organometallic, and materials synthesis.[3] This paper is an account of our efforts to meet these requirements. We first will sketch the basic features of the device to clarify the relationships between the design adaptations and their application. Following this, we will provide a description of the principle of operation of a work-accelerated, electrostatically focused electron gun. The information should be of interest to those unfamiliar with this technique of vaporization. This description will be followed by an evaluation of various electron gun characteristics, including power requirements and charged particle emissions. Our findings should be compared with those given by Green et al.[2] for static reactor systems. The paper concludes with some applications of the device in metal atom synthesis. Additional applications related more to materials science are elaborated in an article by Andrews.[3]

2. Elements of Electron Gun Design

Figures 1 and 2 show views of the dual electron gun, which is the subject of this paper.

2.1. Electron Gun Manifold. This manifold houses the cooling water and electrical connections for the electron gun hearths. The manifold is a hollow shaft constructed of highly polished stainless steel and supported rigidly and horizontally by the main flange assembly (Figure 1). An adjustable collar carries the majority of the weight of the gun as illustrated in Figure 1. A Teflon sleeve has been incorporated to allow easy sliding of the gun manifold through the collar to permit adjustments to the length of the gun.

2.2. Hearth Assembly. A detailed section of the dual gun is illustrated in Figure 2. The twin hearth furnace is constructed of copper and stainless steel. The metals to be vaporized are placed on the water-cooled copper hearths (10-mm diameter), which are capable of accepting 5-10 g of material. These hearths are threaded at the base and tighten against O-ring seals. This feature permits easy interchange of hearth designs. High-voltage feedthroughs connect the anodes through a 1-in.-thick glass-filled nylon insulation block. Half of this block provides additional insulation inside of the gun manifold. Vacuum tightness is achieved with O-ring flanges from the hearths to the nylon block, and from the nylon block to the end of the electron gun manifold. All water and electrical feedthroughs to the hearth assembly are electrically insulated from one another within the main electron gun manifold. Electrical and fluid-transfer leads exit collectively through a plastic sleeve in the rear of the unit (Figure 1).

The thoriated tungsten electron emitter filaments (cathodes) are positioned coaxially approximately 9 mm below the top of each hearth. Braided electrical leads pass from medium-current feedthroughs and, via ceramic insulators, make contact with the

[†] University of Toronto.
[‡] AT&T Bell Laboratories.

(1) Klabunde, K. J. *Chemistry of Free Atoms and Particles*; Academic Press: New York, 1980.
(2) Green, M. L. H. *J. Organomet. Chem.* **1980**, *200*, 119. Green, M. L. H.; O'Hare, D. In *High Energy Processes in Organometallic Chemistry*; Suslick, K., Ed.; ACS Symposium Series 333; American Chemical Society: Washington, DC, 1987.
(3) Andrews, M. P. In *Experimental Organometallic Chemistry*; Wayda, A. L., Darensbourg, M. Y., Eds.; ACS Symposium Series 357; American Chemical Society: Washington, DC, 1987.

0020-1669/90/1329-1068$02.50/0

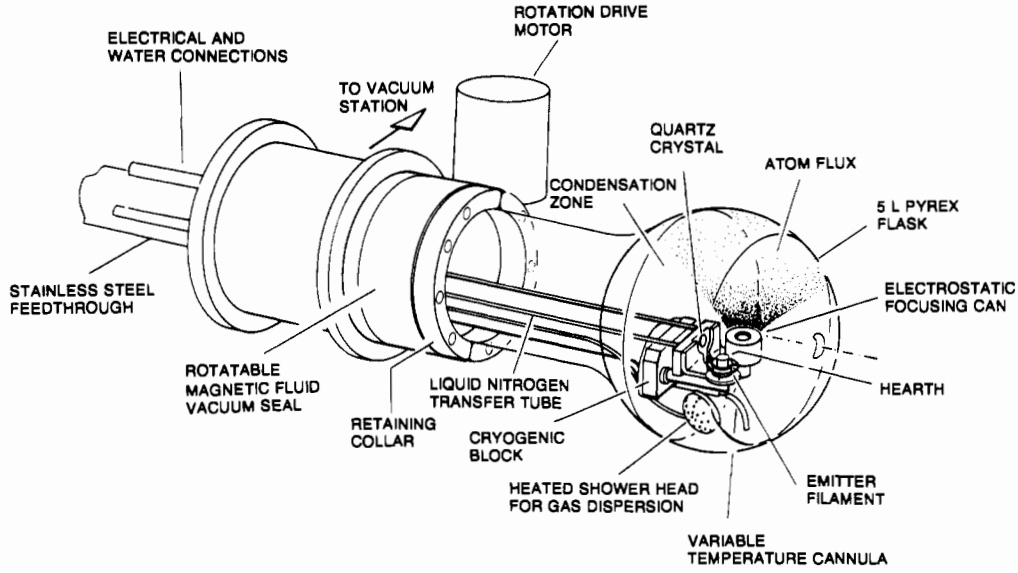

Figure 1. Perspective view of twin positive hearth electrostatically focused electron-beam metal atom reactor.

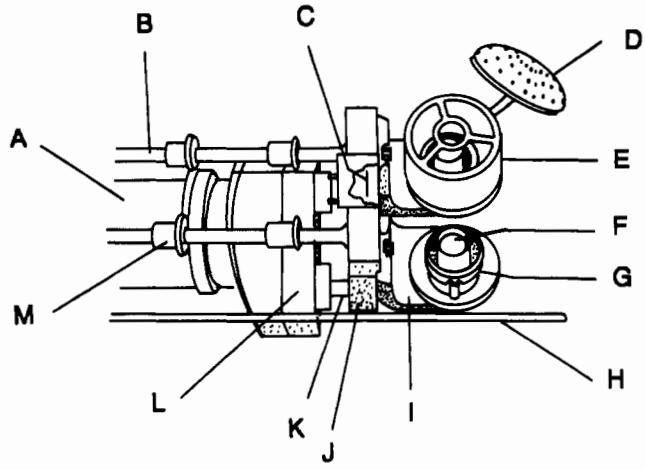

Figure 2. Close-up of twin electrostatic, reverse-polarity electron-beam furnace: (A) stainless-steel shaft housing high/low tension wires and water cooling; (B) liquid-nitrogen- or water-inlet–outlet tube; (C) quartz-crystal mass monitor; (D) heated ligand-inlet shower head with thermocouple monitor; (E) stainless-steel-gauze electrostatic focusing can; (F) water-cooled copper hearth (demountable); (G) thoriated tungsten emitter filament; (H) cannula; (I) adjustable stage for supporting focusing can and emitter filament posts; (J) liquid-nitrogen/water-cooled copper stage; (K) water connection for copper hearth; (L) glass-filled nylon feedthrough; (M) teflon support ring.

filament posts. An electrostatic focusing shield encloses each hearth. The body of these shields is made of a stainless-steel gauze. A satisfactory balance between slightly diminished electron-beam focus and increased usable metal vapor was found by adopting the nearly open can design shown in the sectional perspective of Figure 2.

2.3. Quantitation of Metal Vaporization. By exploitation of the fine mesh construction of the electrostatic focusing shields, a fraction of the high-temperature vapor leaving the hearth can be sampled by a quartz crystal microbalance concealed within the copper support block. The crystal has the property that it can be made to undergo mechanical oscillations when supplied with electrical energy (piezoelectric effect).[4] The resonant oscillation frequency depends on the thickness of the crystal or, alternatively, on the mass of foreign material deposited per unit area on the crystal surface. It can be shown[4,6,7] that the rate of metal deposition is linearly related to the rate at which the oscillation frequency of the crystal decreases. Typically, absolute measurements of areal mass density are accurate to about ±2%. The limit of detection is about 20 ng cm^{-2}. The crystal achieves temperature stability by being part of the liquid-nitrogen- (or water-) cooled block. Quartz crystal wafers cut at the AT angle (35° 20′) are the standard for use as mass monitors because they have the smallest possible temperature coefficient of frequency (related to the crystal elastic constants). Nonetheless, it is noteworthy to protect the crystal against temperature changes due to radiation from the source and the heat of condensation. Heat changes of several degrees Celsius can cause frequency changes of 10–100 Hz. Therefore, the mass monitor is protected by a thin tantalum radiation shield set directly behind the hearths (Figure 2). The thin quartz wafer receives the flux of metal vapor through small holes drilled through the radiation shields. The choice of hole size reflects the desired mass resolution and the temperature coefficient of the crystal for a given metal. The crystal mass monitor therefore provides a means of establishing run-to-run reproducibility in terms of metal atom deposition rate and amount of vaporized metal.

2.4. Vacuum Station and Rotary Drive Mechanism. The high pumping speed that is essential for uninterrupted operation of the electron gun for liquid-phase reactions is provided by a 6-in. VHS 2400 L s^{-1} oil diffusion pump, backed by an Edwards E2M18 direct drive outfit. A 3–25 L Pyrex flask, fitted with a polished 165-mm-o.d. flat glass flange, interfaces with a rotatable, O-ring-grooved stainless-steel flange. The flask is anchored in place by a split-ring collar, which can be bolted to the moving flange. Rotation is achieved by coupling a gear circumscribing the rotatable flange with the worm drive of a Leeson continuous-duty, $^1/_4$-hp drive motor. During rotation, a vacuum of 10^{-7} Torr is guaranteed by a Ferrofluidics magnetic fluid seal. Dynamic vacuum is maintained by pumping through the 5-in.-diameter orifices of two tee flanges that are separated by a butterfly valve. An electropneumatically actuated gate valve isolates a liquid-nitrogen cold trap, which is bolted in place above the diffusion pump.

2.5. Solvent/Solute Transfer. Five $^1/_8$–$^3/_{16}$-in. stainless steel transfer tubes fed through the rear vacuum flange by way of Cajon "Ultra Torr" fittings are located alongside the gun manifold (two of these tubes can be seen in Figure 2). These cannulas are held in the desired position by Teflon–ring-fitted stainless-steel guides attached to the body of the gun. This arrangement permits ample translation and rotation of the tubulations for easy reagent or product transfer. With this arrangement of tubes, solutions and

(4) Stockbridge, C. D. In *Vacuum Microbalance Techniques*; Behrndt, K. H., Ed.; Plenum Press: New York, 1966; Vol. 5.
(5) Unvala, B. A. *Vide* **1963**, *104*, 109.
(6) Eschbah, H. L.; Krindhof, E. W. in *Vacuum Microbalance Techniques*; Behrndt, K. H. Ed.; Plenum Press: New York, 1966; Vol. 5.
(7) Lu, C. S. *J. Vac. Sci. Technol.* **1975**, *12*, 578.

suspensions of solids in fluids can be directed to the desired region of the reaction flask. A heated shower head (Figures 1 and 2) is used to disperse volatile ligands in a uniform band on the inside surface of the Pyrex flask. A Minco Products 60-W button heater attached to the rear of the shower head provides heating sufficient to disperse ligands of low volatility. Temperature changes are detected by an iron–constantan thermocouple set into the base of the shower head.

A variable-temperature solvent/solute transfer tube was developed to conduct thermally unstable materials into or out of the reaction flask. The device is basically a jacketed cannula ($^3/_{16}$-in. i.d. stainless steel) supported by a low/high-temperature fluid vacuum transfer flange. Low-temperature control, for example, is achieved by flowing precooled N_2 gas through the jacket. The temperature of the transfer tube is monitored by means of a chromel–alumel thermocouple attached to the tube at its extreme end inside the reaction vessel. A short length of Teflon tubing equipped with a mechanical manipulator connects the temperature regulated tube with the bottom of the flask.

2.6. Electron Gun Cryopumping. Cryopumping can reduce the vapor pressure in the evaporation zone (hearth area) sufficiently to permit operation of the gun even when high ambient vapor pressures ($>10^{-5}$ Torr) exist in the reaction flask. This is a significant adaptation of the electron gun, since it is otherwise not possible to conduct electron-beam experiments involving volatile liquid solutions in a rotary reactor of this kind. The liquid-nitrogen (or water) cooling to the source assembly can be seen in Figures 1 and 2. Stainless-steel vacuum feedthroughs conduct the coolant through two adjustable-length ($^1/_4$-in-diameter) stainless-steel tubes to the copper block depicted in the perspective of Figure 1. The copper block serves (a) to support the electrostatic focusing shields, (b) to house the quartz-crystal microbalance, and (c) to cryopump the region in the immediate vicinity of the hearths. Additional cryopumping is achieved by attaching a thin foil of stainless steel to the top and sides of the copper cooling block. This shroud also protects the nylon vacuum electrical feedthrough insulation from metal contamination, thereby reducing the possibility of electrical short circuit. The cryopumping capacity of the gun can be further enhanced by expanding the 77 K surface area around the source zone. This is done by wrapping a 10 in. × 3 in. stainless-steel foil about the hearth area, affixing each end to opposite sides of the liquid-nitrogen-cooled block. However, the enhancement in cooling capacity comes at the expense of electron-beam focus, which is degraded because of perturbations in the electrostatic field caused by the presence of the foil.

3. Principle of Operation

The dc circuit is driven by two three-phase (208/220 V) high-voltage (HV) power supplies. These are variable from 0 to 10 kV at 0.2 A. The triphase fullwave rectification produces a dc output voltage with about 14% peak-to-peak ripple, eliminating the need for filter capacitors, which can retain charge. This arrangement is less destructive to the electron gun and safer for the operator. A triac is incorporated to control the input voltage and dc output for each gun. If the current exceeds 0.2 A, the input power is instantaneously cut by a deenergizing self-holding latch in the HV circuit. This event activates an HV circuit breaker to disable the guns. The triac circuit is operated by a 10-V power supply, floated to permit true dc triggering and to shield the triac from false triggers due to transients in the line neutral.

An ac power supply (30 A maximum) provides the filament current to the respective electron guns. The thoriated tungsten filament (General Electric, 1% ThO_2, 0.015-in. diameter) has a work function of about 2.6 eV (those of W and Th are 4.52 and 3.35 eV, respectively). Electrons thermally emitted from the filament find themselves moving along the lines of force curving toward the hearth in the electric field established by the high positive potential at the copper anode. The filament and metal target must be carefully positioned to ensure that the electrons moving in the accelerating potential will converge at a point to surrender their kinetic energy ($E = eU_B$, where U_B is the accelerating voltage) to the metal to give the highest power density. The electrostatic lens is based on one developed originally by Unvala.[5] In his apparatus, both the focusing shield and the filament are held at a high negative potential. Electrons are directed to a grounded target. In our design, components other than the cathode and anode in the hearth area are at or near ground potential. Like the Unvala design, there is no line of sight path for electrons to travel from the filament to the metal target. This arrangement therefore reduces the chances of improper focusing, contamination, and sputtering of the filament by adventitious ions.

The hot emitter filament gives an emission current density I_{em} determined by its temperature and described by the Richardson–Dushman equation, $I_{em} = AT^2 \exp(-B/T)$, where A is the Richardson constant and $B = eU/k$ reflects the work function of the metal (k is Boltzmann's constant). Both A and B depend strongly on the choice of filament material, the most common materials being W, LaB_6, and Ta. The saturation current density of the filament is also affected by the field strength in front of it. Should the field strength be too low to extract the majority of electrons, an electron cloud forms about the filament, and the resulting space charge depresses the cathode emission. Use of small area cathodes generally enhances the space-charge limited current density. There is a transition range between the space-charge and temperature-dependent saturation emission current densities. The cathode is usually operated within this transition to obtain an emission current density at a cathode temperature that is as low as possible.

Since the gun behaves as a diode operating in the saturated regime, the beam current is controlled solely by the electron emission from the filament (i.e., by the filament temperature). Beam focus is rather sensitive to the filament loop diameter and slightly sensitive to the vertical position of the filament. Optimum positioning can be established by trial and error. Additional focusing is achieved by applying a small dc bias to the electrostatic focusing shields. Ideally, all field-influencing components in the construction of the electron gun should observe exact rotational symmetry in order to avoid axial astigmatism.

4. Evaluation of Electron Gun Characteristics Relevant to Metal Vapor Synthesis

To detect the emission of charged particles, the complete source region was surrounded by a collection grid fashioned from wire gauze and connected to a microammeter. The results of these investigations are graphed in Figures 3 and 4 for single and dual electron guns, respectively. The operating powers selected were typical of those used under normal MVS conditions. We have measured rates of metal vaporization, the fraction of metal leaving the hearth, ion- and electron-induced currents for a range of metals, different designs of electrostatic focusing shields, and power levels.

4.1. Charged Particle Emissions. Our results indicated that, for all the transition metals studied, low levels of ions and electrons are emitted. Ion emissions predominate at low accelerating potentials before the metal evaporates, whereas electron emissions are detected at the point of metal vaporization. The shape of these electron–ion emission curves (Figures 3 and 4) is basically the same for all metals investigated, the major distinction being the accelerating potential at which ion emissions occur. The shift to higher accelerating potentials for a given electrostatic focusing shield type is in the same direction as the increase in the heats of sublimation of the various elements. In all cases, rapid increases in ion emissions (0–40 μA) were observed when the metal began to vaporize, and these in fact proved to be excellent indicators of the onset of metal deposition. For working rates of about 1 g h^{-1} we determined that the ratio of metal ion to the neutral metal (M^+/M) was ca. 10^{-4}, which corresponds to ion currents of 40 μA. Note that the curves produced from both the single and dual guns are similar. For the dual electron gun, there was no evidence that the electric field produced by one gun perturbed the other enough to markedly affect the current–voltage, electron, or ion characteristics when both guns were operating simultaneously.

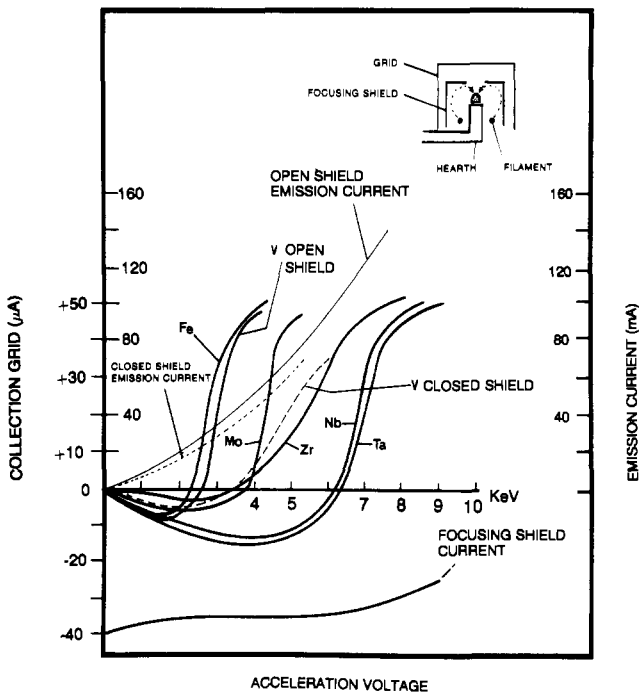

Figure 3. Voltage, current, electron, and ion characteristics of a 10-kV, 200-mA reverse-polarity single electron gun.

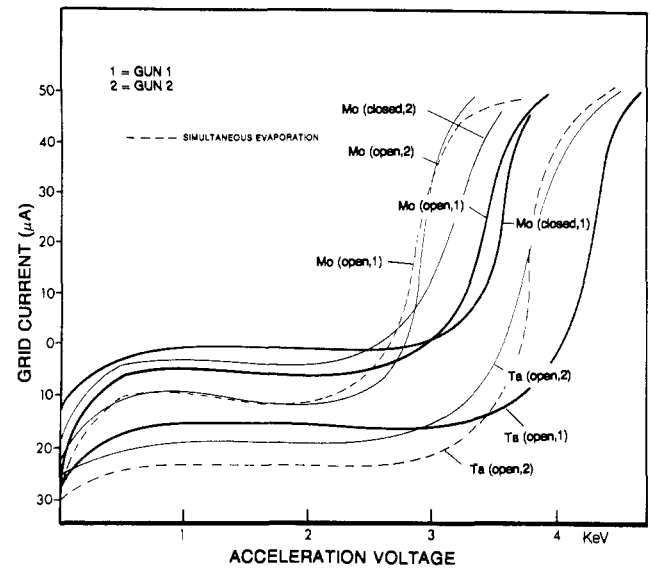

Figure 4. Voltage, current, electron and ion characteristics of a 10-kV, 200-mA reverse-polarity dual electron gun furnace operating singly or simultaneously.

We have found that a solid, metal cylindrical electrostatic focusing shield produces a higher power density (better focus) at the metal target than does a wire-gauze shield, the latter requiring higher operating potentials to reach the same vaporization rate. Superior focusing was also obtained by capping the cylindrical shield with a solid disk having a centered 14-mm aperture to allow atoms to escape; however, such a cap allowed only 40% of the evaporated metal to leave the hearth for reaction. Use of the solid cylindrical shield further reduced the amount of available atoms. We recommend both the wire-gauze shield and the spoked cap for routine use because of the substantial increase in the yield of usable metal vapor. The trade-off in reduced focus by adopting the more open electrostatic focusing shield can be offset by applying a small dc bias (9–50 V) to the shield to collimate the electron beam. The bias also serves to maximize the power density at the target as the button evaporates and diminishes in height.

The similarity of the electron–ion accelerating potential profiles in Figures 3 and 4 can be explained in terms of scattering of the incident electron beam from the metal. This is the origin of the scattered electron emission below the point of metal vaporization. The effect accounts for the minute electron currents (approx. 15 μA, maximum), which are at least 3 orders of magnitude lower than those observed in the earthed hearth mode.[2] Secondary and thermionic electron emission likely persist even at the melting point of the metal.[8] As the primary electron-beam energy increases and the metal begins to evaporate, it is probable that ionizing collisions either in the molten surface regions of the metal or in the gas phase occur to produce small positive ion currents (10–40 μA), for evaporation rates between 0.1 and 1.0 g h^{-1}. The quantity of backscattered electrons and their energy spectrum are determined by the atomic number of the irradiated material and the angle of beam incidence. Reference 9 contains a discussion of these collision processes and their importance in electron-beam technology.

5. Synthetic Applications

The following examples are provided as test applications of the cryopumped electron gun in the liquid-phase synthesis of organometallic compounds from refractory metals.

5.1. Liquid-Phase Reactions. (i) Synthesis of Bis(toluene)vanadium. The metal atom reactor equipped with a 5-L flask was evacuated to 2×10^{-7} Torr. The interior of the gun manifold shaft housing the high tension wires and the cooling water tubes was vigorously purged with dry nitrogen gas to remove condensible water vapor (electric shock and short circuit hazard). This purge was maintained throughout the experiment. Liquid nitrogen was then circulated through the copper block enclosing the hearths of the electron gun. Due to substantial contraction of the metal components comprising the source area, the L-shaped copper stages supporting the focusing shields (Figure 2) shift toward the liquid-nitrogen-cooled copper block, with the result that the hearths and filaments are no longer rotationally symmetric (beam focus is lost). To compensate for this, copper spacers are introduced between the stages and the cold block. A cooling bath (150 K, pentane slush) was elevated around the rotated flask, and a freeze–thaw degassed 10% (v/v) solution of toluene and methylcyclohexane (MCH) was slowly metered into the reactor by a series of valves and cannulas. Cooling water was directed through the hearths and the filament current brought to 20 A. For 30 min, 0.39 g of vanadium was deposited at 2.5 kV and 65 mA. The operating pressure in the flask averaged 5×10^{-6} Torr. On terminating the evaporation, the orange-brown liquid was forced back out of the reactor under a positve pressure of argon. The fluid passed through 1 inch of degassed Celite in a filter frit and collected in a Schlenk tube. The solvent and unreacted toluene were removed under vacuum, and the product was sublimed onto a water-cooled probe at 10^{-3} Torr at room temperature. Yield: 13% based on the amount of vanadium evaporated. Physical properties of bis(toluene)vanadium are described in ref 10.

(ii) Synthesis of Bis(toluene)molybdenum. In a manner similar to that described above, molybdenum atoms were evaporated into toluene–MCH. For this more refractory metal, 2.5 kV at 100 mA emission current was required to vaporize 0.10 g of metal over 30 min. Work up of the products[10] gave 10% bis(toluene)molybdenum based on evaporated Mo.

Thermal conduction and heat radiation strongly determine the efficiency of the melting and evaporation processes. For the refractory elements, high heat losses represent a drawback in the use of water-cooled copper crucibles. Higher powers are required to evaporate a given metal under such conditions. The heat dissipation can be reduced by lining the hearth with a crucible material having poorer thermal conductivity than copper.[3] A carbon liner, 2-mm thick and tightly fitted to the copper hearth to ensure good thermal contact, greatly assists in reducing the

(8) Sommerkamp, P. *Z. Angew. Phys.* **1970**, *28*, 220; Reichelt, W. *Angew. Chem., Int. Ed. Engl.* **1975**, *14*, 218.
(9) Schiller, S.; Heisig, U.; Panzer, S. *Electron Beam Technology*; Wiley: New York, 1982.
(10) Andrews, M. P.; Mattar, S. M.; Ozin, G. A. *J. Phys. Chem.* **1986**, *90*, 1037.
(11) Wilburn, B. E.; Skell, P. *J. Am. Chem. Soc.* **1982**, *104*, 6989.

Table I. Comparisons of Electron Gun Power Required To Evaporate Platinum from Carbon-Lined or Unlined Water-Cooled Copper Hearths

time, h	voltage, kV	current, mA	power, W	mass of Pt vaporized, g
Pt Evaporations Employing a Carbon Liner				
3.0	2.4	68.0	0.163	0.932
4.0	3.5	100.0	0.350	2.033
3.0	3.20	98.0	0.314	0.840
3.5	3.0	99.0	0.297	1.073
Pt Evaporations without a Carbon Liner				
3.5	3.2	85.0	0.272	0.195
3.5	4.5	98.0	0.441	0.253
2.0	4.5	130.0	0.585	0.146

power requirements and improving the yield of atoms from vanadium and molybdenum and very refractory metals like Zr, W, and Pt. In short, we achieve higher evaporation rates at reduced acceleration potentials, for roughly fixed emission current. The level of soft X-ray radiation also diminishes. The overall effect is to reduce the frequency of discharges that shortcircuit the gun, making it easier to conduct vaporizations into organic liquids. Table I compares some results obtained for Pt vaporizations with and without this adaptation. Observe that the introduction of the carbon liner permits substantially more Pt to be evaporated at reduced accelerating potentials and input power. Accordingly, platinum in our hands can be evaporated into MCH solutions for 4 h *without interruption* due to plasma discharges in the reactor.

(iii) Dual-Electron-Beam Vaporization: Single-Step Synthesis of an Organometallic Polymer with Two Different Bound Bis(arene) Transition-Metal Complexes. Titanium and vanadium were incorporated as the polymer-bound sandwich complexes in a liquid poly(dimethyl-*co*-methylphenyl)siloxane as follows: A 5-L Pyrex reaction flask charged with 120 mL of Dow Corning polymer fluid DC510 was bolted onto the rotatable collar of the metal atom reactor. Rough vacuum was first applied gradually to degas the fluid and avoid excessive bumping. When diffusion pumping had brought the system pressure to 2×10^{-6} Torr, an ethylene glycol–water bath (−30 °C) was raised about the slowly rotating flask. Ti and V were evaporated simultaneously into the polymer under 3×10^{-6} Torr vacuum. The current–voltage characteristics for this procedure were as follows: (1) Ti, filament 20 A, hearth 2.0–2.6 kV at 56–80 mA; (2) V, filament 20 A, hearth 2.0–2.4 kV at 75–95 mA. In a 22-min period, 0.128 g (2.56 mmol) of Ti and 0.238 g (4.67 mmol) of V were deposited. The polymer acquired a purple-brown color (bis(arene)titanium complexes are purple). The liquid product was filter-cannulated at room temperature under vacuum onto 2 g of Celite and filtered again under argon to liberate it of particulate metal. The electronic absorption spectrum[9] is displayed in Figure 6. The region of the metal-to-ligand charge-transfer absorption (MLCT) is rather broad owing to the overlap of the 323-nm $(arene)_2V$ MLCT and the $(arene)_2Ti$ MLCT transition at 355 nm. Analysis of the electron spin resonance signal (Figure 5, bottom) gave $g_{av} = 1.987$ and $A_{av} = 63.5$ G, typical for a polymer-bound vanadium sandwich complex.[12]

(iv) Reaction of Mo Atoms with Bis(α,α,α-trifluorotoluene)molybdenum in a Liquid Polymer. The last example illustrates that the liquid-phase electron-beam method can be rather finely tuned to permit reactions between metal atoms and target organometallic compounds in liquid solutions. This experiment is the macrosynthetic scaleup of the Mo + $(CF_3C_6H_5)_2Mo$/DC510 polymer microscale reaction described in ref 13. Thus 0.5 g (2.07 mol) of bis(α,α,α-trifluorotoluene)molybdenum (prepared as described above for Mo and toluene, 47% yield) was dissolved in 15 mL of dry, degassed methylcyclohexane in an Ar-filled drybox. The dark green solution was stirred into 100 mL of thoroughly degassed and dried Dow Corning DC200 liquid polymer. The homogeneous green solution was transferred to a 1-L flask equipped with a Rotaflo stopcock and a conical ground-glass joint. The liquid was again degassed before metering it under vacuum to the rotatable Pyrex reactor flask. Prior to cooling (50:50 ethylene glycol–water), the base pressure registered 3×10^{-6} Torr. Liquid-nitrogen cooling was circulated through the cryogenic block and the emitter filament gradually brought to 20 A. A steady deposition rate of 0.005 mmol h^{-1} was maintained while the flask

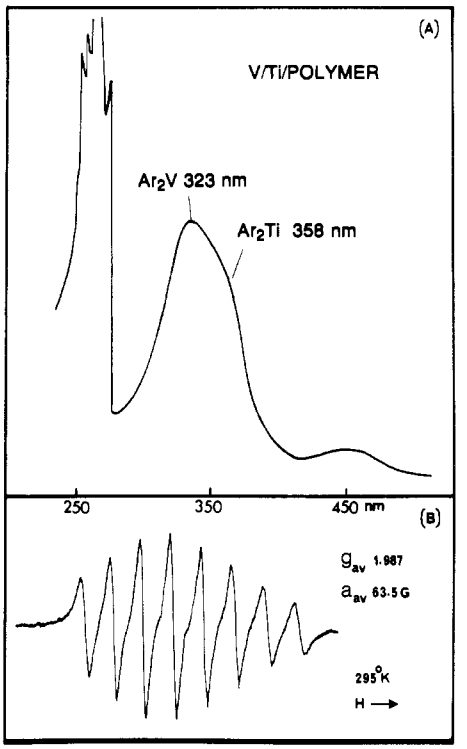

Figure 5. (A) Electronic absorption spectrum of DC510-supported bis(arene)titanium and bis(arene)vanadium. (B) Room-temperature EPR spectrum of the same polymer, approximately 10^{-4} M in the vanadium complex in pentane.

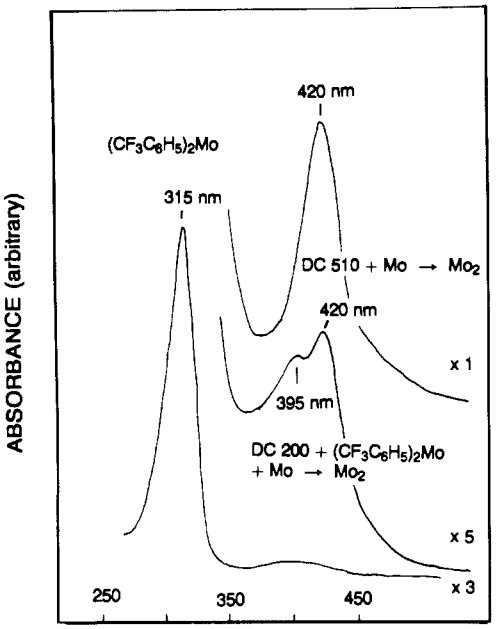

Figure 6. Top: Electronic absorption spectrum attributed to a DC510-supported complex containing two molybdenum atoms (λ_{max} 420 nm), prepared by macroscale electron-beam vaporization of Mo atoms. Middle: Outcome of macroscale electron-beam vaporization of Mo atoms into $(CF_3C_6H_5)_2Mo$ dissolved in DC200. Bottom: Electronic absorption spectrum of $(CF_3C_6H_5)_2Mo$.

(12) Andrews, M. P.; Francis, C. G.; Ozin, G. A. *Inorg. Synth.* **1983**, *22*, 116.
(13) Andrews, M. P.; Ozin, G. A. *Inorg. Chem.* **1986**, *25*, 2587.

was spun at 60 rpm. Slower rotation speeds combined with higher average deposition rates (0.174 mmol h^{-1}) convert the starting material directly to colloid. It was essential in this case to maintain metal atom deposition conditions comparable to those used in the microscale experiments. Note that only a maximum 1.2% conversion of the starting material is expected under the macropreparative conditions.

Mo atoms (0.025 mmol) were deposited at 2.5 kV and 40 mA at 4.5×10^{-6} Torr. The green fluid was transferred cold under Ar backpressure to a Schlenk tube maintained at 77 K. An electronic absorption spectrum was obtained by anaerobic cold transfer of an aliquot of fluid to the 180 K quartz optical window of a cryostat.[3] Figure 6 (bottom) shows the electronic absorption spectrum of the starting bis(α,α,α-trifluorotoluene)molybdenum complex exhibiting absorption maxima at 315 (MLCT) and 395 nm. The middle spectrum for the product of this reaction indicates a new absorption at 420 nm adjacent to the absorption of the starting organometallic target molecule. This band probably owes its origin to a species containing two molybdenum atoms in analogy to the product arising from a similar reaction between Dow Corning 510 fluid and molybdenum atoms.[13]

Acknowledgment. The generous financial assistance of the Natural Sciences and Engineering Research Council of Canada's PRAI and Operating Grants Programs is gratefully appreciated.

Registry No. V, 7440-62-2; Mo, 7439-98-7; $(CF_3C_6H_5)_2Mo$, 82963-88-0; Pt, 7440-06-4; bis(toluene)vanadium, 12131-27-0; toluene, 108-88-3; bis(toluene)molybdenum, 12131-22-5.

Contribution from The Heyrovsky Institute of Physical Chemistry and Electrochemistry, Dolejskova 3, 182 23 Prague 8, Czechoslovakia, and Department of Chemistry and Biochemistry, University of Colorado, Boulder, Colorado 80309-0215

Oxidative Substitution of $Mn(CO)_5^-$ by 3,5-Di-*tert*-butyl-1,2-benzoquinone. Synthesis and Characterization of the Unsaturated $Mn(CO)_3(DBCat)^-$ Anion

František Hartl,† Antonín Vlček, Jr.,*,† Lynn A. deLearie,‡ and Cortlandt G. Pierpont*,‡

Received July 25, 1989

Bu_4N^+ and PPN^+ salts of the $Mn(CO)_3(DBCat)^-$ anion were prepared by oxidative substitution of two CO ligands of $Mn(CO)_5^-$ by 3,5-di-*tert*-butyl-1,2-benzoquinone. The product was characterized by crystallography and by UV-vis, IR, ^{13}C, and ^1H NMR spectroscopy. The complex exhibits some unusual properties: (i) it is a five-coordinate, formally 16-electron, species that shows no tendency to add a sixth ligand, (ii) π-acceptor (CO) and π-donor (catecholate) ligands are combined in the coordination sphere, and (iii) intense LMCT absorption bands are observed. Strong Cat $\rightarrow$ Mn π donation seems to account for this behavior. The complex exhibits two one-electron ligand-localized oxidations at −0.03 and +0.86 V (vs Ag/AgCl) and a one-electron reduction at −1.72 V. The primary product of the first oxidation, $Mn(CO)_3(DBSQ)$, readily coordinates with a donor solvent molecule. Crystals of $Bu_4N^+[Mn(CO)_3(DBCat)]$ form in the triclinic space group $P\bar{1}$ in a unit cell of dimensions a = 10.462 (2) Å, b = 21.629 (4) Å, c = 24.915 (9) Å, α = 102.61 (2)°, β = 93.19 (2)°, γ = 96.87 (2)°, and V = 5443 (2) Å^3. Three crystallographically independent formula units are contained within the asymmetric region of the unit cell. None of the three independent $Mn(CO)_3(DBCat)^-$ anions have regular coordination geometries, but one has a structure that is close to trigonal bipyramidal, while the other two anions have structures that are closer to a square-pyramidal geometry.

Introduction

The photochemical addition of *o*- and *p*-benzoquinones to $Mn_2(CO)_{10}$ has been studied extensively.[1-11] Reaction appears to proceed by addition of the quinone to the photogenerated $Mn(CO)_5$ radical. One-electron oxidative addition gives the six-coordinate semiquinone Mn(I) species $Mn(SQ)(CO)_5$. Oxidation of the metal destabilizes bonding to the carbonyl ligands. When *o*-quinones are used in these reactions, further CO dissociation concomitant with semiquinone chelation leads to the coordinatively saturated $Mn(SQ)(CO)_4$ species. However, these complexes remain susceptible to photochemical CO displacement to give $Mn(SQ)_2$ complexes upon irradiation in the presence of additional *o*-benzoquinone.[4] Catecholate ligands are more effective π donors than the *o*-semiquinones, and there is evidence that chelated catecholate ligands may, synergistically, stabilize the bonding to π acceptors.[12] To investigate this possibility, we have examined the reaction between 3,5-di-*tert*-butyl-1,2-benzoquinone and the $Mn(CO)_5^-$ anion. This reaction might be expected to occur by way of a two-electron oxidative addition process to give the chelated catecholate anion $Mn(DBCat)(CO)_4^-$, with stabilized CO coordination by virtue of catechol π donation. Rather, we have found that the product is the coordinatively unsaturated five-coordinate complex $Mn(DBCat)(CO)_3^-$, formed by further carbonyl displacement. In this report we present details on the synthesis and characterization of the complex.

Results

Formation and Characterization of $Mn(CO)_3(DBCat)^-$. The light yellow color of the CH_2Cl_2 solution of $Mn(CO)_5^-$ immediately turns deep red upon addition of 1 (or less) molar equiv of DBQ.[13] The reaction proceeds without the formation of long-lived intermediates. The 1:1 stoichiometry of the reaction

†The Heyrovsky Institute of Physical Chemistry and Electrochemistry.
‡University of Colorado.

(1) Bowmaker, G. A.; Campbell, G. K. *Aust. J. Chem.* **1979**, *32*, 1897-1904.
(2) Alberti, A.; Camaggi, C. M. *J. Organomet. Chem.* **1979**, *181*, 355-363.
(3) Foster, T.; Chen, K. S.; Wan, J. K. S. *J. Organomet. Chem.* **1980**, *184*, 113-124.
(4) Lynch, M. W.; Hendrickson, D. N.; Fitzgerald, B. J.; Pierpont, C. G. *J. Am. Chem. Soc.* **1981**, *103*, 3961-3963.
(5) Tumanskij, B. L.; Sarbasov, K.; Solodovnikov, S. P.; Budnov, N. N.; Prokofev, A. I.; Kabachnik, M. I. *Dokl. Akad. Nauk SSSR, Ser. Khim.* **1981**, *259*, 611-616.
(6) Sarbasov, K.; Tumanskij, B. L.; Solodovnikov, S. P.; Bubnov, N. N.; Prokofev, A. I.; Kabachnik, M. I. *Izv. Akad. Nauk SSSR, Ser. Khim.* **1982**, 550-555.
(7) Abakumov, G. A.; Cherkasov, V. K.; Shalnova, K. G.; Teplova, I. A.; Razuvaev, G. A. *J. Organomet. Chem.* **1982**, *236*, 333-341.
(8) Vlcek, A., Jr. *J. Organomet. Chem.* **1986**, *306*, 63-75.
(9) Vlcek, A., Jr. *Photochemistry and Photophysics of Coordination Compounds*; Yersin, H., Vogler, A., Eds.; Springer-Verlag: Berlin, Heidelberg, 1987; pp 267-270.
(10) Kaim, W. *Coord. Chem. Rev.* **1987**, *76*, 187-235.
(11) Wang, S. R.; Cheng, C. P.; Ho, I.-I. *J. Chem. Soc., Dalton Trans.* **1988**, 2695-2699.
(12) Shorthill, W. B.; Buchanan, R. M.; Pierpont, C. G.; Ghedini, M.; Dolcetti, G. *Inorg. Chem.* **1980**, *19*, 1803-1805.
(13) Abbreviations used for quinone: DBQ = 3,5-di-*tert*-butyl-1,2-benzoquinone, PQ = 9,10-phenanthrenequinone, CQ = tetrachloro-1,2-benzoquinone. The corresponding catecholate dianions: DBCat, PCat, CCat. Semiquinone radical anions: DBSQ, PSQ, CSQ.

0020-1669/90/1329-1073$02.50/0